Journal of Solid State Chemistry **168,** 34–40 (2002)
doi:10.1006/jssc.2002.9672

# Polymorphism of $IrSn_4$

Eva-Lisa Nordmark, Olle Wallner, and Ulrich Häussermann[1]

*Department of Inorganic Chemistry, Stockholm University, S-10691 Stockholm, Sweden*

Received February 28, 2002

**A high-temperature polymorph of $IrSn_4$ ($\beta$-$IrSn_4$) was prepared from the elements by annealing tin-rich melts at temperatures between 800°C and 900°C and subsequent rapid quenching. The crystal structure of $\beta$-$IrSn_4$ was determined from single-crystal X-ray data (tetragonal, space group $I4_1/acd$, $Z = 8$, $a = 6.3096(6)$ Å, $c = 22.770(7)$ Å) and corresponds to that of $MoSn_4$. In $\beta$-$IrSn_4$, Ir atoms are arranged in layers centering $Sn_8$ square antiprisms. This is in contrast to the trigonal low-temperature modification ($\alpha$-$IrSn_4$) where homogeneously distributed Ir atoms are coordinated in a bisdisphenoidal fashion by eight Sn atoms. The structure of $\beta$-$IrSn_4$, however, is very similar to that of the high-pressure modification of $IrSn_4$ (HP-$IrSn_4$), which adopts the $PtSn_4$ structure. Structural stability of the $IrSn_4$ polymorphs was investigated by first-principles calculations. It was found that $\alpha$-$IrSn_4$ represents the ground state of the system. At ambient pressure $\beta$-$IrSn_4$ is 0.027 eV per formula unit (2.61 kJ/mol) higher in energy than $\alpha$-$IrSn_4$. At a pressure of about 5 GPa, our calculations reveal a phase transition $\alpha$-$IrSn_4 \rightarrow \beta$-$IrSn_4$; the latter remains the most stable polymorph up to pressures of at least 10 GPa. Thus, reported HP-$IrSn_4$ would correspond to a high-pressure–high-temperature form of $IrSn_4$. However, it is suggested that the structures of HP-$IrSn_4$ and $\beta$-$IrSn_4$ are identical.** 

## 1. INTRODUCTION

Stannides of the late transition metals from the Co and Ni groups occur in various compositions and structures (1). The complexity of these systems is partly due to temperature dimorphism, which is a frequent phenomenon among those compounds with a high Sn content (i.e., compounds containing at least 67 at% Sn). The temperature dimorphism of $RhSn_2$ and $PdSn_2$ was studied in detail by Hellner already some 50 years ago (2, 3). More recently, dimorphism was observed for $CoSn_3$ (4) and quasibinary $Co_{1-x}Ni_xSn_2$ ($0.23 < x < 0.59$) (5). Interestingly, for the latter systems a second modification could only be found when synthesis was performed in tin-rich melts thus employing tin as solvent and reactant.

In this work, we report on a high-temperature polymorph of $IrSn_4$ ($\beta$-$IrSn_4$) which was prepared by the quenching of tin-rich melts. The structure of tetragonal $\beta$-$IrSn_4$ is closely related to that of the high-pressure modification of $IrSn_4$ (HP-$IrSn_4$), which crystallizes with the orthorhombic $PtSn_4$ structure type (6). This high-pressure form was the first discovered polymorph of $IrSn_4$. The structure of the trigonal low-temperature form ($\alpha$-$IrSn_4$), which has been published by Lang and Jeitschko (7), is quite different from that of HP-$IrSn_4$ and $\beta$-$IrSn_4$. In order to get some insight into the relative stability of the $IrSn_4$ polymorphs we performed *ab initio* calculations in the framework of density functional theory employing pseudopotentials and a plane wave basis set.

## 2. EXPERIMENTAL SECTION

### 2.1. Synthesis

Starting materials were powders of Ir (ABCR, >99.9%) and Sn (ABCR, >99.999%) which were mixed in a molar ratio of 1:10 thus using Sn as both reactant and flux medium. The reactants were pressed into pellets and loaded into quartz ampoules, which were sealed under vacuum (approx. $10^{-3}$ at). Samples were heated to 400°C, 500°C, 600°C, 700°C, 800°C, and 900°C, annealed for 24 h and subsequently quenched in water. Excess Sn metal was dissolved with 3 M HCl and the remains washed with deionized water. The crystalline products were characterized by Guinier powder diagrams (recorded with Cu$K\alpha$) using Si as internal standard) and by energy disperse X-ray (EDX) analyses in a JEOL scanning microscope.

The 400°C and 500°C samples yielded pure $\alpha$-$IrSn_4$, in accordance with the synthesis by Lang and Jeitschko (7), who used an annealing temperature of 550°C in their preparation of $\alpha$-$IrSn_4$. The 600°C and 700°C samples resulted in pure $Ir_3Sn_7$ with the cubic $Ir_3Ge_7$ structure (8) which was unambiguously identified from the Guinier

[1] To whom correspondence should be addressed. Fax: +46-8-152187. E-mail: ulrich@inorg.su.se.



0022-4596/02 $35.00

powder patterns and EDX compositional analyses. Finally, the 800°C and 900°C samples revealed a mixture of $\beta$-$IrSn_4$ and $Ir_3Sn_7$. The two phases in the crystalline products of those samples could be easily discerned in a stereomagnifier: cubic $Ir_3Sn_7$ crystallizes in block or rod-shaped crystals and $\beta$-$IrSn_4$ in very thin square plates which mostly were found to be grown together to flakes. EDX analyses of such plate-like crystals showed clearly a composition of 20 at% Ir/80 at% without any indication of a homogeneity range.

Plate-like crystals were mechanically separated from the 800°C synthesis sample and ground. The recorded powder diagram could be indexed on the basis of a tetragonal unit cell. The body-centered tetragonal lattice of $\beta$-$IrSn_4$ was later confirmed by the X-ray single-crystal investigation. The lattice parameters of $\beta$-$IrSn_4$ were obtained from least-squares refinements of the measured and indexed lines (program PIRUM (9)). Proper assignment of the indices was ensured by comparing the indices of the observed intensities with the calculated ones (10) using the positional parameters of the single-crystal data refined structure.

**TABLE 1**
**X-Ray Single-Crystal Refinement Data for $\beta$-$IrSn_4$ (the Lattice Parameters Were Obtained from X-Ray Powder Data)**

| | $\beta$-$IrSn_4$ |
|---|---|
| $M_w$ | 666.98 |
| Crystal system | Tetragonal |
| Space group | $I4_1/acd$ |
| Pearson symbol | $tI40$ |
| $a$ (Å) | 6.3096(6) |
| $c$ (Å) | 22.770(7) |
| $V$ (Å$^3$) | 906.5(3) |
| $Z$ | 8 |
| $\rho_{calcd}$ (g cm$^{-1}$) | 9.774 |
| Crystal size (μm$^3$) | $40 \times 40 \times 8$ |
| Transmission (max : min) | 4.57 |
| $\mu$ (mm$^{-1}$) | 50.78 |
| $2\theta$ range $hkl$ | 6.7–56.2 |
| Index range $hkl$ | $-8 \le h \le 8$ |
| | $-8 \le k \le 8$ |
| | $-29 \le l \le 29$ |
| Total no. reflections | 3629 |
| Independent reflections | 283 |
| $R_{int}$ | 0.0694 |
| Reflections with $I > 2\sigma(I)$ | 208 |
| No. of variables | 13 |
| Final $R$ indices [$I > 2\sigma(I)$] | $R = 0.0288$ |
| | $wR = 0.0744$ |
| $R$ indices (all data) | $R = 0.0386$ |
| | $wR = 0.0843$ |
| Largest diff. peak/hole (eÅ$^{-3}$) | 2.07/−2.80 |

[a] $R_1 = \sum ||F_o| - |F_c|| / \sum |F_o|$.
[a] $wR_2 = \left(\sum[w(F_o^2 - F_c^2)^2] / \sum[w(F_o^2)^2]\right)$.
$w = 1/[\sigma^2(F_o^2) + (aP)^2 + bP]$ and $P = F_o^2 + 2F_c^2/3$.
$a = 0.0533$, $b = 18.54$.

**TABLE 2**
**Atomic Position Parameters, Site Occupancies, and Isotropic Thermal Displacement Parameters for $\beta$-$IrSn_4$**

| Atom | $I4_1/acd$ | $x$ | $y$ | $z$ | s.o.f. | $U_{eq}$ |
|---|---|---|---|---|---|---|
| Ir | 8b | 0 | 0.25 | 0.125 | 1 | 74(3) |
| Sn | 32g | 0.17292(9) | 0.57660(9) | 0.06143(2) | 1 | 103(3) |

*Note.* $U_{eq}$ ($\times 10^4$ Å$^2$) is defined as one-third of the trace of the orthogonalized $U_{ij}$ tensor.

## 2.2. Structure Determination

Intensity data of a $\beta$-$IrSn_4$ single crystal (selected from the 800°C sample) was collected at room temperature on a STOE IPDS system (11) using rotating anode generated monochromatized Mo$K\alpha$ radiation (0.71073 Å). A numerical absorption correction was performed with the program X-shape (12).

The centrosymmetric space group $I4_1/acd$ was assigned on the basis of the systematic absences and the statistical analysis of the intensity distributions. The structure was determined from Patterson syntheses (program SHELXS97 (13)) and refined against $F^2$ with the program SHELXL97 (14). Some details of the single-crystal data collection and refinement are listed in Table 1. Atomic position parameters and selected interatomic distances are given in Tables 2 and 3, respectively. Further details of the crystal structure investigation may be obtained from Fach in formations zentrun karlsruhe, D-76344 Eggenstein-Leopoldshafen, Germany (fax: (+49) 7247-808-666; e-mail: crysdata@fiz-karlsruhe.de) on quoting the depository number CSD-412573.

## 2.3. Electronic Structure Calculations

Total energy calculations for $IrSn_4$ were performed within *ab initio* density functional theory as implemented in the program VASP (15). Concerning the pseudopotentials, ultrasoft Vanderbilt-type pseudopotentials (16) were employed considering 5*d* and 6*s* electrons as valence electrons for Ir and 4*s* and 4*p* electrons as valence electrons for Sn. We considered $IrSn_4$ in the structure types $IrGe_4$ ($\alpha$-$IrSn_4$), $MoSn_4$ ($\beta$-$IrSn_4$), $PtSn_4$ (HP-$IrSn_4$), and $PtPb_4$. For all structures, atomic position parameters and lattice parameters were relaxed for a set of constant volumes until forces had converged to less than 0.01 eV/Å. In a second step, we extracted equilibrium volume $V_{eq}$ and corresponding energy $E_{eq}$ of each polymorph by fitting the obtained $E$ vs $V$ values to a Birch–Murnaghan equation of state. The exchange and correlation energy was assessed by the generalized gradient approximation (GGA) (17). Convergency of the calculations was checked with respect to the plane wave cutoff and the number of $k$ points used in the

**TABLE 3**
**Comparison of Interatomic Distances (Å) in α- and β-$IrSn_4$**

| α-$IrSn_4$ (Ref. (7)) | | | | β-IrSn4 | | | |
|---|---|---|---|---|---|---|---|
| Ir | 2 | Sn1 | 2.705 | Ir | 4 | Sn | 2.745 |
| | 2 | Sn1 | 2.746 | | 4 | Sn | 2.748 |
| | 2 | Sn3 | 2.739 | | | | |
| | 2 | Sn2 | 2.864 | | | | |
| Sn1 | 1 | Ir | 2.705 | Sn | 1 | Ir | 2.745 |
| | 1 | Ir | 2.746 | | 1 | Ir | 2.748 |
| | 1 | Sn3 | 2.962 | | 1 | Sn | 2.962 |
| | 1 | Sn2 | 3.134 | | 1 | Sn | 3.090 |
| | 1 | Sn2 | 3.135 | | 1 | Sn | 3.203 |
| | 1 | Sn3 | 3.230 | | 2 | Sn | 3.300 |
| | 1 | Sn1 | 3.320 | | 2 | Sn | 3.301 |
| | 2 | Sn1 | 3.339 | | | | |
| Sn2 | 2 | Ir | 2.864 | | | | |
| | 2 | Sn2 | 3.047 | | | | |
| | 1 | Sn3 | 3.114 | | | | |
| | 2 | Sn1 | 3.134 | | | | |
| | 2 | Sn1 | 3.135 | | | | |
| Sn3 | 2 | Ir | 2.739 | | | | |
| | 2 | Sn2 | 2.962 | | | | |
| | 1 | Sn1 | 3.114 | | | | |
| | 2 | Sn2 | 3.230 | | | | |

*Note*. Only distances shorter than 3.6 Å are listed. Standard deviations are all equal or less than 0.001 Å.

summation over the Brillouin zone. Concerning the plane wave cutoff, a energy value of 300 eV was chosen. $K$ points were generated by the Monkhorst–Pack method (18) and sampled on grids $4 \times 4 \times 4$ ($MoSn_4$ structure), $6 \times 6 \times 6$ ($IrGe_4$ structure), and $8 \times 8 \times 8$ ($PtSn_4$ and $PtPb_4$ structures). The integration over the Brillouin zone was performed with a Gaussian smearing of 20 mRy.

## 3. RESULTS AND DISCUSSION

### 3.1. Crystal Structures of α-$IrSn_4$ (LT) and β-$IrSn_4$ (HT)

α-$IrSn_4$ is formed from tin-rich melts at temperatures lower than 600°C. Its crystal structure is isotypic to trigonal $IrGe_4$ (space group $P3_121$, $Z = 3$) and consists of one kind of Ir atom (Wyckoff position 3*b*) and three different kinds of Sn atoms (Wyckoff positions 6*c* (Sn1) and two types 3*a* (Sn2, Sn3)). The Ir atoms are coordinated by eight Sn atoms forming a distorted bisdisphenoid (triangle dodecahedron). The $IrSn_8$ coordination polyhedron represents the basis unit for a simple and beautiful description of the α-$IrSn_4$ structure (Fig. 1). We first note that four of the eight bisdisphenoid vertices correspond to Sn1 atoms and the remaining four are divided among two Sn2 and Sn3 atoms (Fig. 1a). In α-$IrSn_4$, bisdisphenoids are fused via a pair of oppositely situated (not connected) Sn2–Sn3 edges which yields chiral polyhedra strands (Fig. 1b). The translational period of a strand contains three polyhedra and the translational direction coincides with the $c$ direction in the α-$IrSn_4$ structure. Next, bisdisphenoid strands are connected to the neighboring ones by exclusively sharing Sn1 corners (Fig. 1c). Thus, all Sn atoms belong to two $IrSn_8$ coordination polyhedra: Sn2 and Sn3 atoms are shared between two neighboring

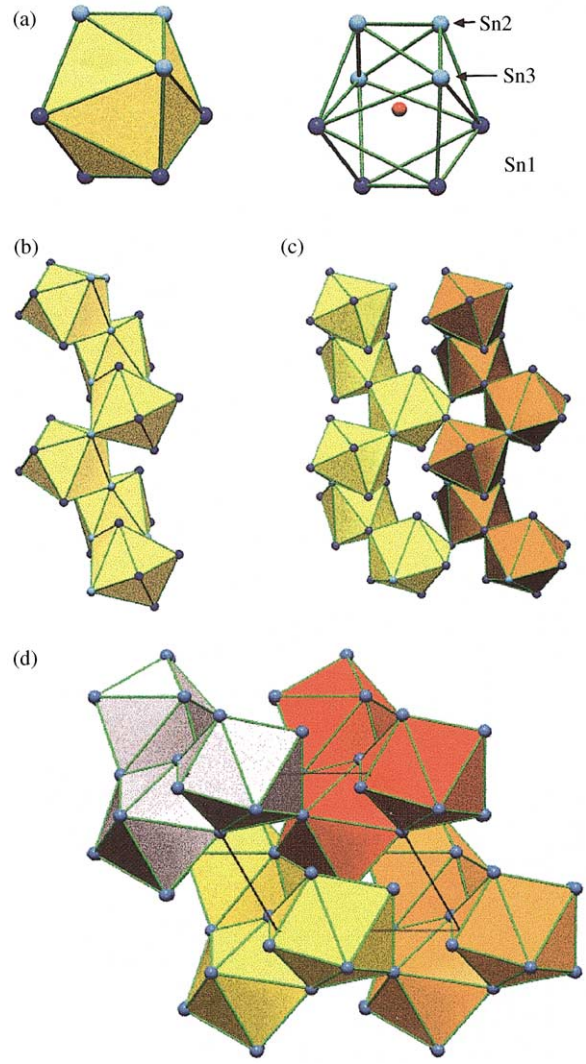


**FIG. 1.** Description of the crystal structure of trigonal α-$IrSn_4$ ($IrGe_4$ type). (a) The bisdisphenoid coordination polyhedron of Ir defined by $4 \times$ Sn1, $2 \times$ Sn2 and $2 \times$ Sn3 (blue and green circles denote Sn atoms, red circles correspond to Ir atoms). (b) Bisdisphenoids are fused into strands by sharing a pair of oppositely situated (not connected) Sn2–Sn3 edges. (c) Neighboring strands are connected by sharing Sn1 vertices. (d) A view of total structure of α-$IrSn_4$ along [001] showing the arrangement of strands in the unit cell. The polyhedral strands are symmetrically equivalent but distinguished by different colors.

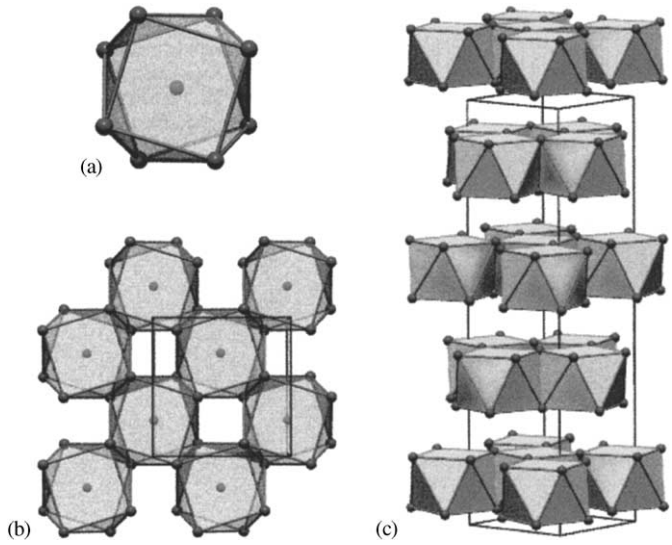


**FIG. 2.** Description of the crystal structure of tetragonal $\beta$-$IrSn_4$ ($MoSn_4$ type). (a) The square antiprism coordination polyhedron of Ir. (b) $IrSn_8$ square antiprisms form a layer by sharing common edges. In $\beta$-$IrSn_4$ such layers are stacked in an *ABCD* sequence along the *c* direction. (c) View of the total structure approximately along [110].

polyhedra within a strand and all Sn1 atoms are shared between polyhedra of neighboring strands, which yields the stoichiometry $IrSn_{8/2} = IrSn_4$. In the hexagonal unit cell of trigonal $\alpha$-$IrSn_4$ polyhedra strands run along the cell axis [001]; each strand is surrounded by six symmetry equivalent ones and Fig. 1d shows the total structure of $\alpha$-$IrSn_4$ projected along [001].

$\beta$-$IrSn_4$ is formed from tin-rich melts at temperatures higher than 700°C. Its crystal structure is isotypic to tetragonal $MoSn_4$ (space group $I4_1/acd$, $Z = 8$) and consists of one kind of Ir atom (Wyckoff position 8*b*) and one kind of Sn atoms (Wyckoff position 32*g*). $\beta$-$IrSn_4$ is only the second representative of the recently discovered $MoSn_4$ structure type (19). The Ir atoms of $\beta$-$IrSn_4$ are coordinated by eight Sn atoms forming a square antiprism (Fig. 2a). Such $IrSn_8$ units are further arranged into layers by sharing common edges (Fig. 2b). In tetragonal $\beta$-$IrSn_4$ layers are stacked in an *ABCD* sequence along the *c* direction. This view of the total structure is shown in Fig. 2c.

Apart from the same coordination number of the Ir atoms there is no relation between the structures of $\alpha$- and $\beta$-$IrSn_4$. Characteristic for both structures is that direct Ir–Ir contacts are avoided (the closest Ir–Ir distance in $\alpha$-$IrSn_4$ is 4.65 Å and in $\beta$-$IrSn_4$ 4.22 Å). Somewhat unusual, the volume of the high-temperature modification (113.31 $Å^3/Z$) is slightly lower (by 0.8%) than that of the low-temperature form (114.17 $Å^3/Z$). Interatomic distances in the $IrSn_4$ temperature dimorphs are compared in Table 3. The distances Ir–Sn in $\alpha$-$IrSn_4$ range from 2.71 to 2.86 Å, whereas in $\beta$-$IrSn_4$ they are confined to 2.75 Å. The mean distances, however, are very similar (2.764 and 2.746 Å for $\alpha$- and $\beta$-$IrSn_4$, respectively). The Sn atom in $\beta$-$IrSn_4$ exhibits a similar nearest neighbor distance distribution as the Sn1 atom in $\alpha$-$IrSn_4$.

### *3.2. Structural Variations Based on the $3^2434$ Net*

The $MoSn_4$-type structure of $\beta$-$IrSn_4$ can be embedded into a family of related structures which are realized by intermetallic *TE* compounds (*T* = transition metal, *E* = *p*-block element). For this purpose, we first consider the $CuAl_2$ structure. In the $CuAl_2$ structure, Al atoms form $3^2$ 434 nets (Fig. 3a) which are stacked exactly on top of each other. This leads to an assembly of rows of face-sharing square antiprisms which are centered by the Cu atoms (Fig. 3b). Upon removing every second (001) layer of Cu atoms, the composition is changed to *TE* and layers of edge-sharing $CuAl_8$ centered square antiprisms remain, i.e., the building block of the $MoSn_4$ structure. These layers are situated in the same orientation on top of each other yielding a stacking sequence *AA*. This is the structure of $PtPb_4$ (Fig. 3c) (20). When considering the $PtPb_4$ structure as an aristotype, more structures can be derived by applying crystallographic shearing (21) to the $PtPb_4$ layers. Layers might be shifted by the vectors $(\frac{1}{2}, 0)$, $(0, \frac{1}{2})$, or $(\frac{1}{2}, \frac{1}{2})$ in the (00 l) planes. The effect of the shear operations is demonstrated in Figs. 3d and 3e. The shifts $(\frac{1}{2}, 0)$ and $(0, \frac{1}{2})$ create an antiphase boundary with respect to the neighboring $3^2434$ nets of two adjacent $PtPb_4$ layers, (Fig. 3d). The shift $(\frac{1}{2}, \frac{1}{2})$ transforms neighboring $3^2434$ nets of two adjacent $PtPb_4$ layers, which are oriented in antiposition, into the same orientation (Fig. 3e).

The structure of $PtSn_4$ (22) arises from the $PtPb_4$ structure when applying $(\frac{1}{2}, 0)$ shifts as shearing operation to every second $PtPb_4$ layer (Fig. 3f). This yields a stacking sequence $A_{(0,0)}B_{(1/2,0)}$, where the shift vector relative to *A* is specified in subscripts, accompanied with a doubling of the *c*-axis. The shift $(\frac{1}{2}, 0)$ destroys the 4-fold axis in the *c* direction and the resulting arrangement has orthorhombic symmetry with ideally the *a*- and *b*-axis being of the same length. However, for the representatives with the $PtSn_4$ structure (1) (e.g., $PtSn_4$, $PdSn_4$, $AuSn_4$, and HP-$IrSn_4$) the short orthorhombic axes differ slightly in length (up to 1%).

The structure of $MoSn_4$ (19) results from the $PtPb_4$ structure when applying the sequence of shifts $(0,0) \rightarrow (\frac{1}{2}, 0) \rightarrow (\frac{1}{2}, \frac{1}{2}) \rightarrow (0, \frac{1}{2})$ to four consecutive layers yielding the stacking sequence $A_{(0,0)}B_{(1/2,0)}C_{(1/2,1/2)}D_{(0,1/2)}$ (Fig. 3g). Consequently, the *c*-axis is quadrupled with respect to the parent $PtPb_4$ structure (and doubled with respect to the $PtSn_4$ structure). Importantly, this sequence of shifts introduces $\bar{4}$, $4_1$, and $4_3$ axes in the stacking direction, which retains the tetragonal symmetry.

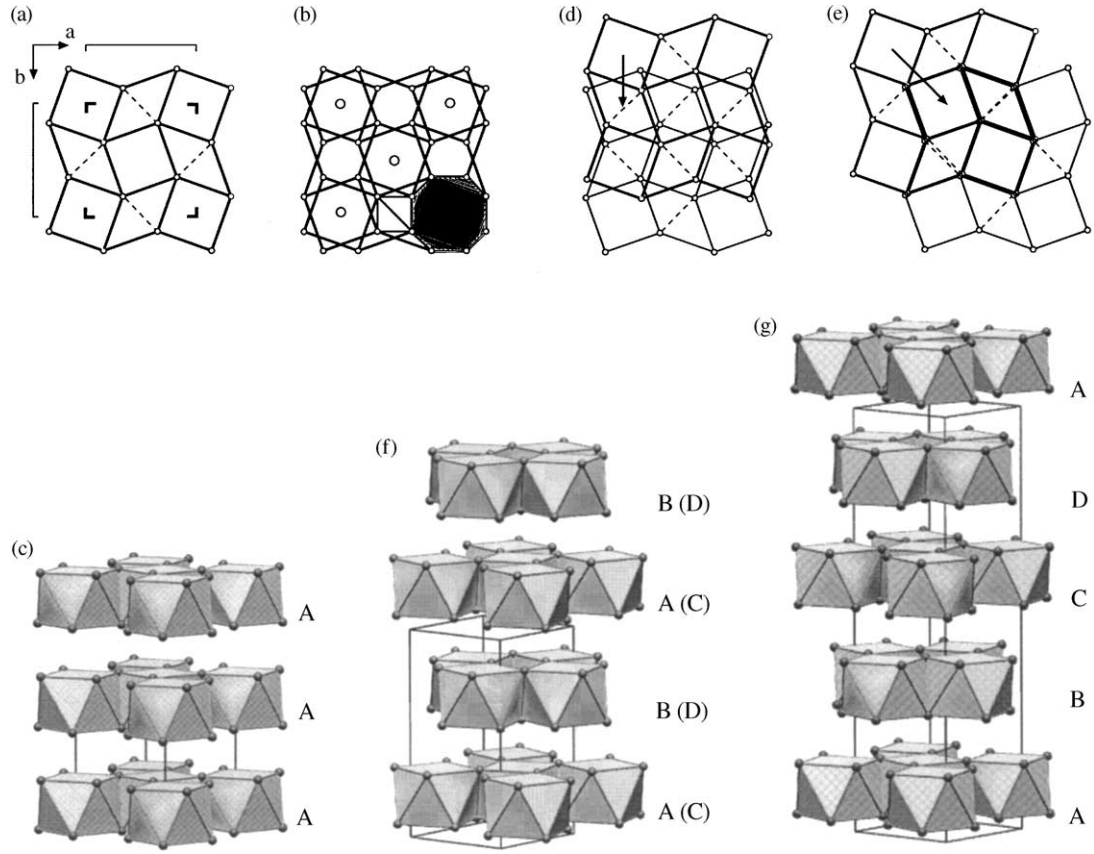


**FIG. 3.** (a) The square $3^2$ 434 net consisting of diamonds and squares. (b) The $CuAl_2$ structure consisting of rows of face-sharing centered square antiprisms (circles in the net corners denote A1 atoms; circles in the center of the antiprisms represent Cu atoms). (c) The tetragonal $PtPb_4$ structure with an *AA* stacking of building blocks (gray circles denote Pb atoms). The application of crystallographic shear operations to a sequence of two $3^2$ 434 nets: (d) translation $(0,\frac{1}{2})$ and (e) translation $(\frac{1}{2},\frac{1}{2})$. (f) The orthorhombic $PtSn_4$ structure with an *AB* stacking of building blocks. (In this figure, the square antiprismatic layers appear in the *C*- and *D*-type orientation when taking the orientation of layers in the $PtPb_4$ structure as a reference (*A*)). (g) The tetragonal $MoSn_4$ structure with an *ABCD* stacking of building blocks.

The outlined mechanism of crystallographic shearing for deriving intermetallic *TE* structure types applies as well to other building blocks than a single square antiprismatic layer (defined by two consecutive $3^2$434 nets). For example, a building block consisting of a double layer of centered square antiprims (defined by three consecutive $3^2$ 434 nets) can be used to derive the structures of $PdSn_3$ (23) and $\beta$-$CoSn_3$ (i.e., the temperature dimorphs of $CoSn_3$ (4)). Note that the composition now is $TE_3$; the square antiprism centering *T* atoms form pairs with short contacts. In the $PdSn_3$ structure, the building blocks are $A_{(0,0)}$ $B_{(1/2,0)}$ stacked and in the $\beta$-$CoSn_3$ structure the sequence $A_{(0,0)}B_{(1/2,0)}C_{(1/2,1/2)}D_{(0,1/2)}$ is realised. Thus, this pair of structures is related in the same way as is the pair $PtSn_4$/$MoSn_4$. More examples for building blocks are described in Ref. (5); additionally this reference addresses the problem of stacking faults and microtwinning, which especially affects the orthorhombic *AB* stacked variants.

### 3.3. Structural Stability of the $IrSn_4$ Polymorphs

The lower volume per formula unit of $\beta$-$IrSn_4$ compared to $\alpha$-$IrSn_4$ could rise the suspicion that perhaps $\beta$-$IrSn_4$ is the actual ground state of $IrSn_4$ and its exclusive formation from high-temperature melts is due to kinetic reasons. Additionally, besides the described temperature dimorphs there exists HP-$IrSn_4$, the high-pressure modification with the $PtSn_4$ structure type (6). This polymorph was obtained from a stoichiometric sample at pressures above 6 GPa and temperatures of 520–720°C. In order to settle the question of the ground state structure of $IrSn_4$ and to get some insight into the high-pressure behavior of this system, we performed first-principles calculations within density functional theory. In particular, we computed the total energy of $IrSn_4$ in the structure types $IrGe_4$, $MoSn_4$, $PtSn_4$, and $PtPb_4$ as a function of volume. This included a complete relaxation of all structural

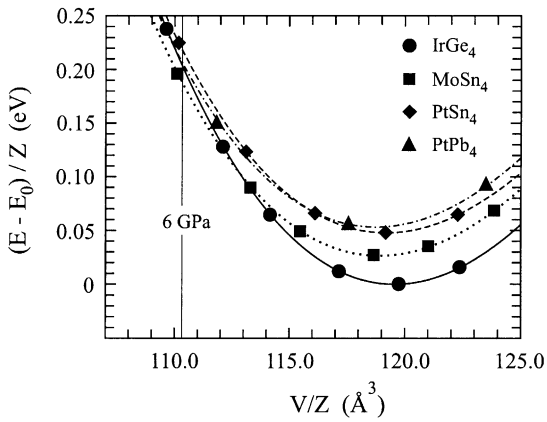


**FIG. 4.** Calculated energy vs volume for $IrSn_4$ in the structure types $IrGe_4$ ($\alpha$-$IrSn_4$, circles–solid line), $MoSn_4$ ($\beta$-$IrSn_4$, squares–dotted line), $PtSn_4$ (diamonds–dashed line), and $PtPb_4$ (triangles–dash–dotted line). $E_0$ is the energy of the calculated equilibrium volume of ground state $\alpha$-$IrSn_4$. The vertical line inserted indicates the pressure applied for the synthesis of HP-IrSn4 (6 GPa) (6).

parameters. These results are summarized in Fig. 4 and Table 4.

We first focus on structural competition at ambient pressure, i.e., the comparison of the total energies corresponding to the equilibrium volumes. From Fig. 4, it is clearly seen that $\alpha$-$IrSn_4$ indeed represents the ground state of $IrSn_4$. Its total energy at equilibrium volume is 0.027 eV/$Z$ (2.61 kJ/mol) lower than that of $\beta$-$IrSn_4$. The total energies of the $PtSn_4$- and $PtPb_4$- type polymorphs are very close to each other, but these polymorphs are at least 0.021 eV/$Z$ higher in energy than $\beta$-$IrSn_4$. In Table 4, we compare the experimental structural parameters of $\alpha$- and $\beta$-$IrSn_4$ with the computationally modelled ones. The absolute values of the equilibrium volumes obtained by theory are overestimated by about 5%. This overestimation of equilibrium volumes is frequently observed when using GGA for assessing exchange and correlation energy. However, the volume difference between $\alpha$- and $\beta$-$IrSn_4$ is correctly reproduced. Further, the $c/a$ parameters and atomic position parameters are in excellent agreement with the experimentally obtained ones.

Next, we turn to the high-pressure behavior of $IrSn_4$. Upon volume reduction (pressure increase), the total energy of $\alpha$-$IrSn_4$ increases more than the ones of the layered structures. Thus, $\alpha$-$IrSn_4$ has a higher bulk modulus (calculated value: 79 GPa) and is less compressible than the layered structure polymorphs. The latter attain a very similar value for the bulk modulus (around 70 GPa). Supposing that in $IrSn_4$, the main bonding contribution arises from the interaction between Ir $d$ and Sn $p$ states, the $IrSn_8$ polyhedra represent rather tightly bonded entities. Thus, the stiffer behavior of $\alpha$-$IrSn_4$ compared to the layered structure polymorphs is simply a consequence of the homogeneous distribution of $IrSn_8$ polyhedra in its crystal structure. Further, the combination of a higher equilibrium volume and a higher bulk modulus of ground state $\alpha$-$IrSn_4$ compared to the layered structure polymorphs gives rise to a structural transition under pressure. Our calculations reveal a transition $\alpha$-$IrSn_4$ ($IrGe_4$ type)$\rightarrow$ $\beta$-$IrSn_4$ ($MoSn_4$ type) at a pressure of 4.9 GPa. This finding agrees partly with the synthesis of HP-$IrSn_4$ at 6 GPa (and elevated temperatures). However, the reported structure for HP-$IrSn_4$ is $PtSn_4$ which would be the least stable $IrSn_4$ polymorph at this pressure (cf. Fig. 4) and thus would correspond to a high-pressure–high-temperature modification of $IrSn_4$. Since the published X-ray powder intensity data for HP-$IrSn_4$ (6) (taken at ambient pressure) are rather incomplete and $IrSn_4$ in the $ABCD$ stacked $MoSn_4$ and the $AB$ stacked $PtSn_4$ structure yields a very similar powder pattern, it might be possible that the structures of $\beta$-$IrSn_4$ and HP-$IrSn_4$ actually are identical ($MoSn_4$ type).

## 4. CONCLUSIONS

A high-temperature form of $IrSn_4$ ($\beta$-$IrSn_4$) was synthesized from the elements by annealing tin-rich melts at temperatures above 700°C and subsequent rapid quench-

**TABLE 4**
**Comparison of the Structural Parameters of $\alpha$- and $\beta$-$IrSn_4$ Obtained from Theory and Experiment**

| | $V_{eq}$/Z (Å$^3$) | $c/a$ | $x_{Ir}$ | $x_{Sn1}$ | $y_{Sn1}$ | $z_{Sn1}$ | $x_{Sn2}$ | $x_{Sn3}$ |
|---|---|---|---|---|---|---|---|---|
| $\alpha$-$IrSn_4$ | Trigonal | | | | | | | |
| Theory | 119.53 | 1.263 | 0.3105 | 0.2350 | 0.4977 | 0.4323 | 0.0903 | 0.6310 |
| Exp.[a] | 114.17 | 1.262 | 0.3112 | 0.2333 | 0.4982 | 0.4330 | 0.0898 | 0.6312 |
| $\beta$-$IrSn_4$ | Tetragonal | | | | | | | |
| Theory | 118.83 | 3.583 | | 0.1725 | 0.5765 | 0.0622 | | |
| Exp.[b] | 113.31 | 3.608 | | 0.1729 | 0.5766 | 0.0614 | | |

[a] Ref. (7).
[b] This work.

ing. The structure of tetragonal $\beta$-$IrSn_4$ was found to be isotypic to the hitherto unique $MoSn_4$ type and thus is quite different from the structure of trigonal low-temperature $\alpha$-$IrSn_4$. In $\alpha$-$IrSn_4$, Ir atoms are coordinated in a bisdisphenoidal fashion by Sn atoms and the $IrSn_8$ polyhedra are homogeneously distributed in the crystal structure. In $\beta$-$IrSn_4$, the coordination polyhedron of Ir corresponds to a square antiprism and the $IrSn_8$ polyhedra are connected into layers. With the aid of crystallographic shearing, the $MoSn_4$ structure of $\beta$-$IrSn_4$ can be nicely related to the ones of $PtPb_4$ and $PtSn_4$. The three structures represent stacking variants of the same building block. The $PtSn_4$ type has been considered as the structure of the high-pressure modification of $IrSn_4$. However, according to our first-principles calculations this polymorph is not the most stable at high pressures but would be high-temperature $\beta$-$IrSn_4$.

## ACKNOWLEDGMENT

This work was supported by the Swedish Research Council (VR).

## REFERENCES

1. P. Villars and L. D. Calvert, "Pearsons Handbook of Crystallographic Data of Intermetallic Phases," 2nd ed. American Society for Metals, Materials Park, OH, 1991, and Desk Edition, 1997.
2. E. Hellner, *Z. Kristallogr.* **107,** 99 (1956).
3. E. Hellner, *Z. Kristallogr.* **107,** 124 (1956).
4. A. Lang and W. Jeitschko, *Z. Metallkd.* **87,** 759 (1996).
5. U. Häussermann, A. R. Landa-Cánovas, and S. Lidin, *Inorg. Chem.* **36,** 4307 (1997).
6. V. I. Larchev and S. V. Popova, *J. Less-Common Met.* **98,** L1 (1984).
7. A. Lang and W. Jeitschko, *J. Mater. Chem.* **6,** 1897 (1996).
8. O. Nial, Svensk Kemisk Tidskrift **59,** 172 (1947).
9. P.-E Werner, *Ark. Kemi* **31,** 513 (1969).
10. Lazy-Pulverix, K. Yvon, W. Jeitschko, and E. Parthé, *J. Appl. Crystallogr.* **10,** 73 (1977).
11. "IPDS (Version 2.87)," Stoe and Cie GmbH, Darmstadt, Germany, 1996.
12. "XSHAPE: Crystal Optimisation for Numerical Absorption Correction," Stoe and Cie GmbH, Darmstadt, Germany, 1996.
13. G. M. Sheldrick, *Acta Crystallogr. A* **46,** 467 (1990).
14. G. M. Sheldrick, "SHELXL97," University of Göttingen, Germany, 1997.
15. (a) G. Kresse and J. Hafner, *Phys. Rev. B* **47,** RC558 (1993); (b) G. Kresse and J. Furthmüller, *Phys. Rev. B* **54,** 11169 (1996).
16. (a) D. Vanderbilt, *Phys. Rev. B.* **41,** 7892 (1990); (b) G. Kresse and J. Hafner, *J. Phys.: Condens. Matter* **6,** 8245 (1994).
17. J. P. Perdew and Y. Wang, *Phys. Rev. B* **45,** 13244 (1992).
18. H. J. Monkhurst and J. D. Pack, *Phys. Rev. B* **13,** 5188 (1976).
19. V. Kuntze, H. Hillebrecht, and Y. Grin, "VIth European Conference on Solid State Chemistry", Zürich, Switzerland, 1997.
20. U. Rösler and K. Schubert, *Naturwissenschaften* **38,** 331 (1951).
21. B. G. Hyde and S. Andersson, "Inorganic Crystal Structures," John Wiley & Sons, New York, 1989.
22. U. Rösler and K. Schubert, *Z. Metallkd.* **41,** 298 (1950).
23. K. Schubert, H. L. Lukas, H.-G. Meissner, and S. Bhan, *Z. Metallkd.* **50,** 534 (1959).